Phase slips in coupled oscillator systems

Pragjyotish Bhuyan Gogoi,[1] Suresh Kumarasamy,[2] Awadhesh Prasad,[1] and Ram Ramaswamy[3]
[1]*Department of Physics and Astrophysics, University of Delhi, Delhi 110007, India*
[2]*Centre for Computational Modelling, Chennai Institute of Technology, Chennai 600069, India*
[3]*Department of Chemistry, Indian Institute of Technology Delhi, New Delhi 110016, India*

(Received 1 May 2023; accepted 7 July 2023; published 28 July 2023)

Phase slips are a typical dynamical behavior in coupled oscillator systems: the route to phase synchrony is characterized by intervals of constant phase difference interrupted by abrupt changes in the phase difference. Qualitatively similar to stick–slip phenomena, analysis of phase slip has mainly relied on identifying remnants of saddle-nodes or "ghosts." We study sets of phase oscillators and by examining the dynamics in detail, offer a more precise, quantitative description of the phenomenon. Phase shifts and phase sticks, namely, the temporary locking of phases required for phase slips, occur at stationary points of phase velocities. In networks of coupled phase oscillators, we show that phase slips between pairs of individual oscillators do *not* occur simultaneously, in general. We consider additional systems that show phase synchrony: one where saddle-node ghosts are absent, one where the coupling is similarity dependent, and two cases of coupled chaotic oscillators.

DOI: 10.1103/PhysRevE.108.014209

I. INTRODUCTION

Of the various forms of synchronization [1–3] that are known to occur in coupled dynamical systems, phase synchrony—when the amplitudes of oscillation are uncorrelated but the phases are identical [4–7]—is one of the simplest. Recognized as a weak form of synchrony between two coupled systems [4–6], phase synchronization is widely observed in lasers [8], Josephson junctions [9,10], neurons [11,12], electronic circuits [13,14], cardiac and respiratory rhythms [15], brain dynamics [12,16], ecological systems [17], or camphor ribbons [18,19], for example. In recent years, growing interest in networks of coupled oscillators has further extended its domain [6,20], and now phase synchronization has been observed in networks of coupled chaotic oscillators [21], delay-coupled chemical oscillators [22], networks of phase oscillators [23,24], coupled map networks [25], flow models of production networks [26], and networks of bursting neurons [27]. Making extensive use of phase oscillator models [28–30], the concept of phase synchronization has been utilized in complex networks for purposes of control, with applications in vehicle coordination [31–33] and designing power networks [34,35].

The manner in which two coupled oscillators can phase synchronize has been studied in some detail, and it appears that near the onset of phase synchrony, the dynamics shows a phase version of stick–slip dynamics [5,36]: the dynamics of the oscillators becomes highly correlated, the phase difference becomes constant for a time interval, changes rapidly, becomes constant again, and so on. Qualitatively, this corresponds to alternating periods of synchrony with brief intermediate periods of asynchrony between the two oscillators. The role of ghost points, namely, remnants of saddle nodes [36,37] in effecting phase slippage, has also been explored in some detail. Our goal here is to analyze, in continuation with previous works [2,6,29], aspects of phase synchronization that have remained relatively unexplored, such as the temporal relationship between phase slips in individual oscillators and the locations of the slips in coupled systems.

In the present paper, we show that phase slips occur when the dynamics in the phase space of the system is at stationary points of the flow *velocities*. Consider a general n-dimensional dynamical system

$$\dot{\mathbf{X}} = \mathbf{F}(\mathbf{X}), \tag{1}$$

where $\mathbf{X}$ is the vector $(x_1, x_2, \ldots, x_n)^\intercal$ and $\mathbf{F} \equiv (F_1(\mathbf{X}), \ldots, F_n(\mathbf{X}))^\intercal$, a stationary point in the state space, $\mathbf{X}^{pp} \equiv (x_1^{pp}, x_2^{pp}, \ldots, x_n^{pp})^\intercal$, such that

$$\ddot{x}_i(\mathbf{X}^{pp}) = 0, \quad i = 1, 2, \ldots, n, \tag{2}$$

namely,

$$\sum_{j=1}^{n} \dot{x}_j \cdot \frac{\partial F_i}{\partial x_j}\bigg|_{\mathbf{X}=\mathbf{X}^{pp}} = 0, \quad i = 1, 2, \ldots, n \tag{3}$$

is termed a perpetual point [38]. These are distinct from fixed points of the flow, namely, those that satisfy

$$\dot{x}_i(\mathbf{X}) = 0, \quad i = 1, 2, \ldots, n, \tag{4}$$

and appear to determine the occurrence of phase slippage.

The concept of perpetual points is relatively new, and has been introduced to recognize a class of points complementary to fixed points with potentially comparable relevance [38]. These have been seen to be useful as a tool to locate hidden attractors [39–41], which are known not to be associated to any fixed points, in continuous as well as discrete-time systems [38,42]. They find applications in mechanical systems in understanding rigid body motion and energy dissipation [43,44] and help regulate the dynamics of slow-fast oscillations, bursting, canards, or mixed-mode behavior [45]. Perpetual points are moreover essential in understanding

systems with prolonged transient dynamics such as neural processing, transient chaos, and ecology [38,46,47].

In the following Sec. II, we consider the Kuramoto model [28,45] of two coupled phase oscillators, where we carry out the analysis in detail and show how this extends to the cases of three or more oscillators. We consider different coupling forms in Sec. III; the analysis carries over for the case of extended coupling as well as when the coupling is modulated by a similarity-dependent term [48]. In Sec. IV, we consider chaotic systems for further generalization. We conclude the paper with a discussion and summary in Sec. V.

II. COUPLED PHASE OSCILLATORS

Since our focus is on phase dynamics, we consider a system of n phase oscillators with the nearest coupling [36,45],

$$\dot{\theta}_i = \omega_i + \frac{\varepsilon}{2}[\sin(\theta_{i+1} - \theta_i) + \sin(\theta_{i-1} - \theta_i)] \quad i = 1, \ldots, n, \tag{5}$$

where the θ_i's are the oscillator phases, ω_i's the oscillator frequencies, and ε is the coupling strength. We analyze the cases for $n = 2$, 3 and for a network of oscillators.

A. The $n = 2$ case

For $n = 2$, namely,

$$\begin{aligned} \dot{\theta}_1 &= \omega_1 + \varepsilon \sin(\theta_2 - \theta_1), \\ \dot{\theta}_2 &= \omega_2 + \varepsilon \sin(\theta_1 - \theta_2), \end{aligned} \tag{6}$$

a change of variables to $\phi = \theta_2 - \theta_1$ and $\psi = \theta_2 + \theta_1$ is convenient since clearly $\dot{\psi} = (\omega_1 + \omega_2)$ is conserved. The approach to synchrony can be gauged via the nontrivial dynamics

$$\dot{\phi} = \Delta\omega - 2\varepsilon \sin\phi, \tag{7}$$

where $\Delta\omega = \omega_2 - \omega_1$.

For illustration purposes, we take $\omega_1 = 1$, $\omega_2 = -2$, so $\Delta\omega = -3$. When $\varepsilon > |\Delta\omega|/2$, there are two fixed points that exist at $\phi = \sin^{-1}(\Delta\omega/2\varepsilon)$ (stable) and $\phi = \pi - \sin^{-1}(\Delta\omega/2\varepsilon)$ (unstable). These are indicated in Fig. 1(a) for the case $\varepsilon = 1.55$. The stable fixed point (FP_1, the closed circle) is at $\phi \approx 4.96$ and the unstable one (FP_2, the open circle) at $\phi \approx 4.46$. Independent of the initial values of θ_1 and θ_2, the system always reaches the phase-locked state at FP_1. For the individual oscillators, this implies reaching a synchronous state wherein their phase difference remains locked even though the phases themselves evolve. The extrema of $\dot{\theta}_1$ and $\dot{\theta}_2$, namely, $\ddot{\theta}_1 = -\ddot{\theta}_2 = 0$ occur when $\phi = \pi/2, 3\pi/2$ and are marked by the two filled black squares (P_1 and P_2) in Fig. 1(a). These are the perpetual points (PPs) of the system.

The two stationary points move towards each other when ε is decreased, and when $\varepsilon = |\Delta\omega|/2$, they annihilate each other at a saddle-node bifurcation. The perpetual points continue to exist [see Fig. 1(b) for $\varepsilon = 1.45$] and these now dictate the dynamics of the system. Phase-slips occur, as illustrated in the evolution of ϕ, shown in Fig. 2(a) (the dashed red line): the variation is stepwise, consisting of recurring flat segments connected by short, steep portions. The nearly constant values of ϕ, indicative of temporary phase locking between the oscillators occur around P_2 ($\phi = \frac{3\pi}{2}$). Since the magnitude of $\dot{\phi}$ is minimum here ($\sim$0.1), ϕ varies slowly and the system dynamics is sticky in the vicinity of P_2. A stroboscopic map of the dynamics is shown in Fig. 2(b), where $\sin\phi$ is plotted versus $\cos\phi$ at equal intervals of time; the high concentration of points near P_2 indicates the long time spent in its vicinity. As the system moves away from P_2, both oscillators speed up by equal amounts, since $\dot{\theta}_1 + \dot{\theta}_2$ is constant. This makes the magnitude of $\dot{\phi}$ large ($\sim$5.9) as the system nears the fast perpetual point P_1 located at $\phi = \frac{\pi}{2}$. At P_1, the oscillators move with the maximum possible speeds in opposite directions and the system rapidly experiences a substantial change in ϕ. As can be seen in Fig. 2(a) $\dot{\phi}$ vs t (solid curve) displays a trough each time the system passes through P_1. The corresponding dips in ϕ are apparent in the ϕ vs t (dashed) curve: these sudden changes are the phase slips and signify the maximal asynchrony between the oscillators [36].

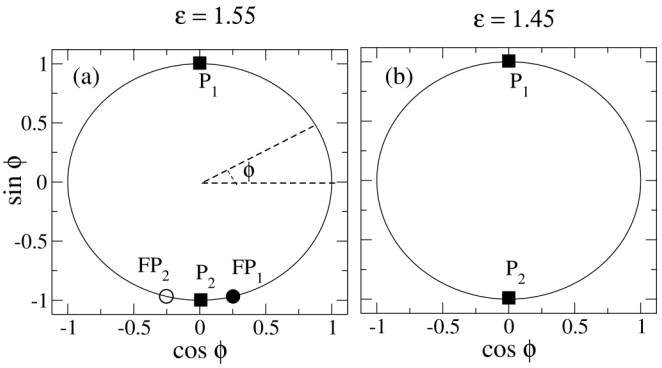

FIG. 1. Schematic representation of the unstable (open circle) and stable (closed circle) fixed points, and the perpetual points (filled squares) for the choice of parameters $\omega_1 = 1$, $\omega_2 = -2$ in Eq. (7). (a) For $\varepsilon = 1.55 > |\Delta\omega|/2$, there are two fixed points (FP_1 and FP_2) and two perpetual points (P_1 and P_2), and (b) the slow (P_2) and the fast (P_1) perpetual points when $\varepsilon = 1.45 < |\Delta\omega|/2$.

As ε is decreased further, the velocity differential between the perpetual points drops and phase slips become less prominent. This can be seen in the sequence of ϕ vs t curves in Fig. 3(a), and the corresponding $\dot{\phi}$ vs t curves in Fig. 3(b), for $\varepsilon = 1.45$, 1 and 0.5. The extent of these phase slips can be measured by the ratio

$$\rho = \frac{t_S}{T}, \tag{8}$$

where T is the time period of oscillations and we define t_S as the time spent around the slow perpetual point P_2 [see Fig. 2(b)]; we define t_S as the time taken for the half-oscillation passing through P_2, namely, the time taken for the orbit to go from $\cos\phi = 1$ to $\cos\phi = -1$. In terms of the phase, this is the time spent in the interval $\pi + 2k\pi \leqslant \phi \leqslant 2(k+1)\pi$, with integer k. If $\rho \approx 1$, then most of the time is spent around the slow point P_2 and the phase slips are prominent. On the other hand, if the motion is uniform, $\rho = \frac{1}{2}$, and the phase slips are not visible. In Fig. 4, ρ is plotted as a function of $|\Delta\omega| - 2\varepsilon$, which is the distance from the saddle-node bifurcation point for Eq. (7). When the separation is small, $\rho \sim 1$, and therefore the phase slips are

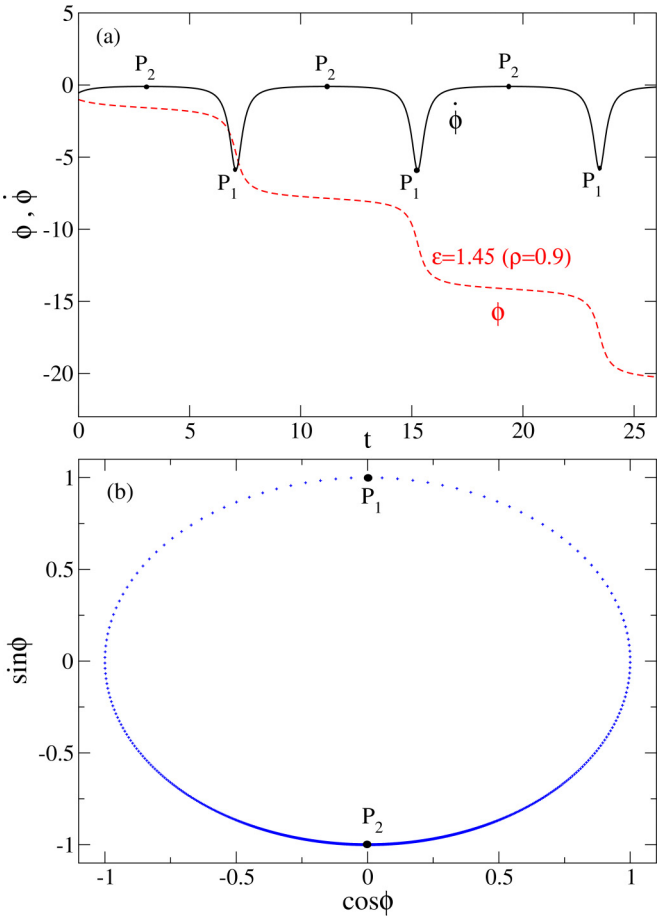

FIG. 2. For the case of $n = 2$ and $\varepsilon = 1.45$, namely, Eq. (7), (a) the phase difference, ϕ (dashed red), and velocity, $\dot{\phi}$ (solid black) as a function of time, and (b)a plot of $\sin\phi$ vs $\cos\phi$. The points in (b) are equally spaced in time, showing the difference in the dynamics near the fast point P_1 and the slow point P_2.

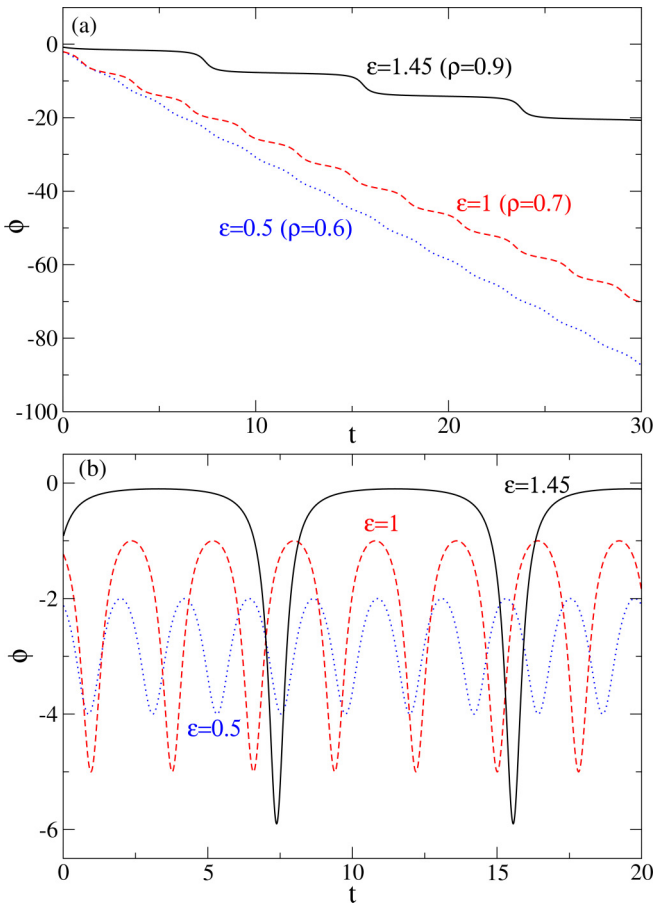

FIG. 3. Also, for $n = 2$ [see Eq. (7)], (a) the variation of ϕ with time for $\varepsilon = 0.5$ (dotted blue), $\varepsilon = 1$ (dashed red), and $\varepsilon = 1.45$ (solid black). The phase slips become more visible with increasing ε. The phase velocity is shown for the same ε values in (b), with the velocity at P_2 (the peaks of the curves) approaching zero as ε increases.

clearly visible—see Figs. 2(a) and 3(a). As the distance from the bifurcation point increases, ρ decreases, making the phase slips less apparent, as can also be seen in Fig. 3(a).

It can be shown that proximity to the ghost of the saddle-node bifurcation is not a necessary condition for the phase slip. Consider, for example, the modified phase velocity equation

$$\dot{\phi} = \delta + \varepsilon \sin^2\phi, \tag{9}$$

where δ is the distance from the ghost point and ε is now the velocity difference between the corresponding perpetual points $P_1(\phi = \frac{\pi}{2}$, fast) and $P_2(\phi = 0$, slow) of this system. Defining T and t_S as before, we compute ρ as a function of ε for different δ; this is shown in Fig. 5(a). Far from the saddle-node bifurcation, it is possible to have ρ close to 1 for large enough ε. For instance, the phase slip structure for $\delta = 7$ with $\varepsilon = 200$ is shown in Fig. 5(b); the corresponding value of ρ is 0.9.

We thus see that perpetual points give insight into the dynamics during phase slippage, and provide a way to identify the exact locations of the slips.

B. *n* oscillators in a ring

1. n = 3

The equations of motion for $n = 3$ oscillators with periodic boundary conditions are

$$\begin{aligned}
\dot{\theta_1} &= \omega_1 + \frac{\varepsilon}{2}(\sin(\theta_2 - \theta_1) + \sin(\theta_3 - \theta_1)),\\
\dot{\theta_2} &= \omega_2 + \frac{\varepsilon}{2}(\sin(\theta_1 - \theta_2) + \sin(\theta_3 - \theta_2)),\\
\dot{\theta_3} &= \omega_3 + \frac{\varepsilon}{2}(\sin(\theta_1 - \theta_3) + \sin(\theta_2 - \theta_3)).
\end{aligned} \tag{10}$$

Defining $\phi_{ij} = \theta_j - \theta_i$ and $\Delta\omega_{ij} = \omega_j - \omega_i$, one can easily obtain the equivalent set of equations

$$\begin{aligned}
\dot{\phi}_{12} &= \Delta\omega_{12} + \frac{\varepsilon}{2}(-2\sin\phi_{12} + \sin\phi_{23} + \sin\phi_{31}),\\
\dot{\phi}_{23} &= \Delta\omega_{23} + \frac{\varepsilon}{2}(-2\sin\phi_{23} + \sin\phi_{31} + \sin\phi_{12}),\\
\dot{\phi}_{31} &= \Delta\omega_{31} + \frac{\varepsilon}{2}(-2\sin\phi_{31} + \sin\phi_{12} + \sin\phi_{23}),
\end{aligned} \tag{11}$$

describing the relative dynamics between individual oscillators. Note that since $\phi_{12} + \phi_{23} + \phi_{31} = 0$, one can get the

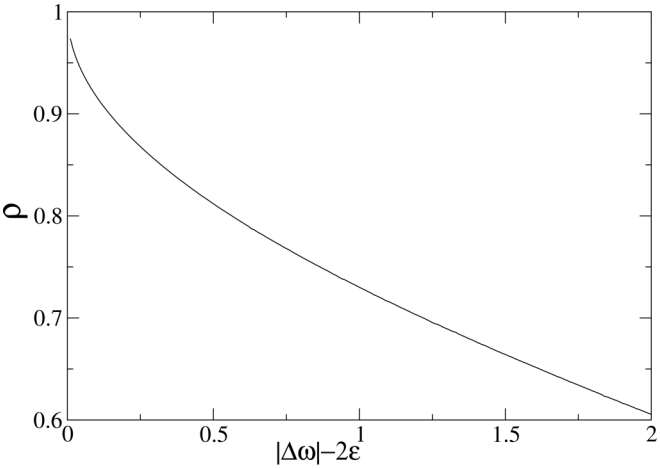

FIG. 4. The extent of the phase-slip ρ as a function of the offset, $|\Delta\omega| - 2\varepsilon$. This calculation uses Eq. (7) with $\Delta\omega = -3$.

reduced set of equations

$$\dot{\phi}_{12} = \Delta\omega_{12} + \frac{\varepsilon}{2}(-2\sin\phi_{12} + \sin\phi_{23} - \sin\phi_{123}),$$
$$\dot{\phi}_{23} = \Delta\omega_{23} + \frac{\varepsilon}{2}(-2\sin\phi_{23} + \sin\phi_{12} - \sin\phi_{123}), \quad (12)$$

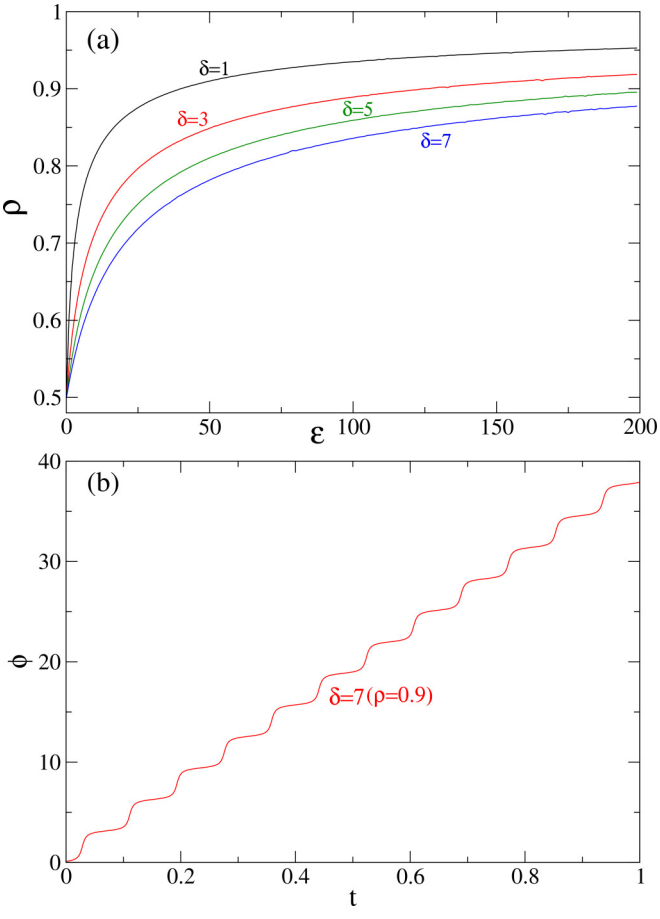

FIG. 5. For the modified phase velocity function Eq. (9), extent of the phase slip ρ as a function of ε for different δ in (a), and (b) the phase ϕ as a function of time for $\delta = 7$, far from the saddle-node ghost, with $\varepsilon = 200$.

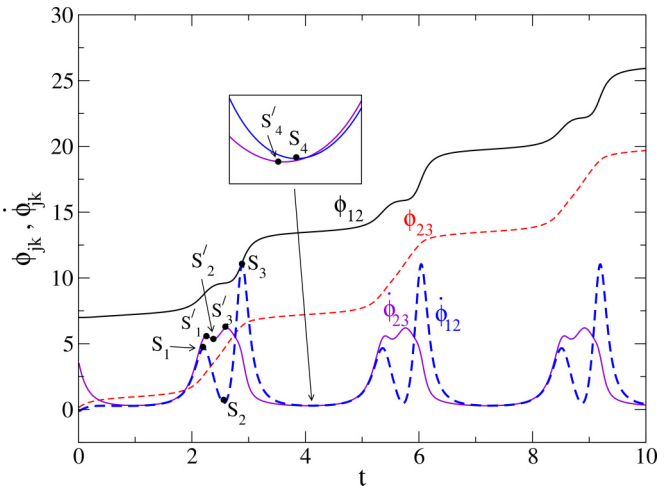

FIG. 6. Plots of $\dot{\phi}_{12}$ (dashed blue) and $\dot{\phi}_{23}$ (solid violet) as a function of time for Eq. (12) with $\Delta\omega_{12} = 4.3$, $\Delta\omega_{23} = 4.2$, and $\varepsilon = 4.5$. The stationary points for $\dot{\phi}_{12}$ are marked S_1, S_2, S_3, and S_4, and those for $\dot{\phi}_{23}$ are marked S'_1, S'_2, S'_3, and S'_4. The corresponding phase-slip structures can be seen in the ϕ_{12} (solid black) and ϕ_{23} (dashed red) curves.

where $\phi_{123} \equiv \phi_{12} + \phi_{23}$. Perpetual points are simultaneously the extrema of $\dot{\phi}_{12}$ and $\dot{\phi}_{23}$, and it is straightforward to show that at such points, the condition

$$\dot{\phi}_{12}\cos\phi_{12} = \dot{\phi}_{23}\cos\phi_{23} = -\dot{\phi}_{123}\cos\phi_{123} \quad (13)$$

holds.

For arbitrary $\Delta\omega_{12}$, $\Delta\omega_{23}$, this condition is not easily satisfied, so perpetual points are uncommon. Thus, in general, phase slips in ϕ_{12} and ϕ_{23} will not occur simultaneously, as shown in the example in Fig. 6 for $\Delta\omega_{12} = 4.3$ and $\Delta\omega_{23} = 4.2$, with $\varepsilon = 4.5$. There are four stationary points each for $\dot{\phi}_{12}$ and $\dot{\phi}_{23}$, indicated as S_k and S'_k, $k = 1, \ldots, 4$ in Fig. 6. The slips occur at S_1, S_3, S'_1, and S'_3, while around S_4 and S'_4 the dynamics is sticky. Asynchrony between phase slips is also observed in coupled map systems [49].

If we set $\Delta\omega_{12} = \Delta\omega_{23}$, Eq. (12) is invariant under the interchange $\phi_{12} \leftrightarrow \phi_{23}$, so in this case the variables $\dot{\phi}_{12}$ and $\dot{\phi}_{23}$ evolve identically. The stationary points of the velocities are therefore identical and can be recognized as perpetual points, the locations of which are easily determined as

$$P_1 : (|\cos^{-1}\alpha| \pm 2k\pi, |\cos^{-1}\alpha| \pm 2l\pi),$$
$$P_2 : (|\cos^{-1}\beta| \pm 2k\pi, |\cos^{-1}\beta| \pm 2l\pi),$$
$$P_3 : (-|\cos^{-1}\beta| \pm 2k\pi, -|\cos^{-1}\beta| \pm 2l\pi),$$
$$P_4 : (-|\cos^{-1}\alpha| \pm 2k\pi, -|\cos^{-1}\alpha| \pm 2l\pi),$$

where $\alpha = (-1 + \sqrt{33})/8$, $\beta = (-1 - \sqrt{33})/8$, and k, l are integers, *independent* of $\Delta\omega_{12}$ and $\Delta\omega_{23}$. These are marked on Fig. 7 for $\Delta\omega_{12} = \Delta\omega_{23} = 1$, $\varepsilon = 1.13$, and, as can be seen, the slips in ϕ_{12} (solid-black curve) and ϕ_{23} (dashed-red curve) occur simultaneously at points P_2 and P_4.

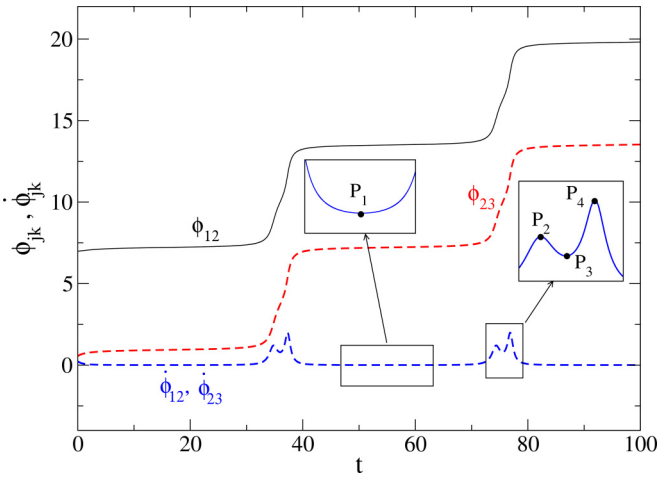

FIG. 7. Plot of $\dot\phi_{12}$ and $\dot\phi_{23}$ as a function of time, for Eq. (12) with $\Delta\omega_{12} = \Delta\omega_{23} = 1$ and $\varepsilon = 1.13$ (the dashed-blue curve). Perpetual points are marked P_1, P_2, P_3, and P_4, and the simultaneous phase-slip structures are seen in the ϕ_{12} (solid black) and ϕ_{23} (dashed red) curves.

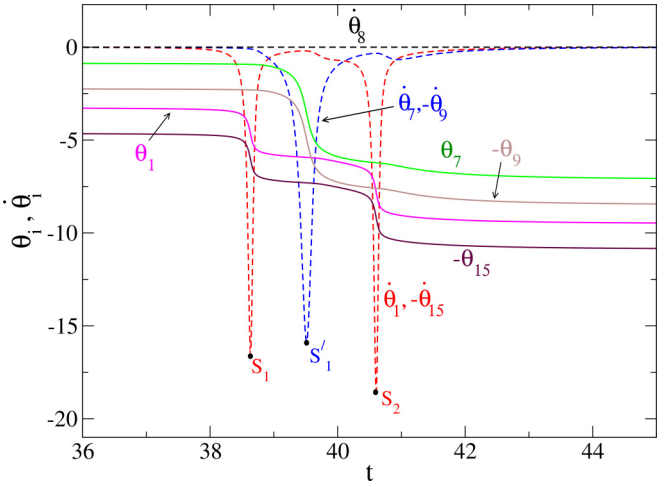

FIG. 9. For the case of $n = 15$ and $\varepsilon = 28$ in Eq. (5), the variation of θ_1 (solid magenta), θ_7 (solid-green), $-\theta_9$ (solid-brown), $-\theta_{15}$ (solid maroon), together with $\dot\theta_1$ (dashed red), $\dot\theta_7$ (dashed blue), $\dot\theta_8$ (dashed black), $-\dot\theta_9$ (dashed blue), and $-\dot\theta_{15}$ (dashed red) as a function of time.

From Eq. (10), using the equality $\sin\phi_{12} = \sin\phi_{23}$, one gets

$$\dot\theta_2 = \omega_2, \tag{14}$$

namely, the angular velocity of the second oscillator is constant, independent of ε, and therefore so is the sum $\dot\theta_1 + \dot\theta_3$. When ε is increased, the velocities of the other two oscillators approach ω_2, see Figs. 8(a)–8(d). Synchronization is reached once they equal ω_2. The ϕ_{12} vs t (solid black) and ϕ_{23} vs t (dashed red) curves in Fig. 7 capture the relative motion of θ_1 and θ_3 with respect to θ_2 near synchronization.

Similar to the case discussed in the previous section, the relative dynamics of the oscillators can be analyzed using the perpetual points. Figure 7 shows that maximum time is spent around the perpetual point with the global velocity minimum

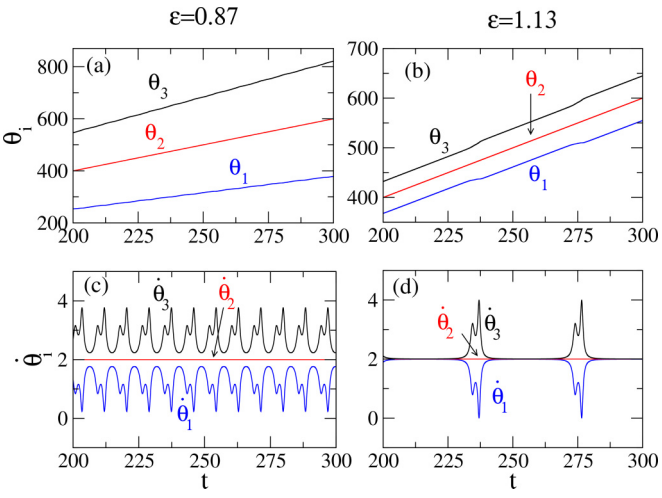

FIG. 8. For Eq. (10) with $\omega_1 = 1$, $\omega_2 = 2$, and $\omega_3 = 3$, the phases, θ_1 (solid blue), θ_2 (solid red), and θ_3 (solid black) at (a) $\varepsilon = 0.87$, and (b) $\varepsilon = 1.13$ and phase velocities $\dot\theta_1$, $\dot\theta_2$, and $\dot\theta_3$ at (c) $\varepsilon = 0.87$ and (d) $\varepsilon = 1.13$.

(P$_1$), while slips occur at the fast perpetual points (P$_2$ and P$_4$). The dynamics at P$_1$ in this case corresponds to maximum alignment of $\dot\theta_1$ and $\dot\theta_3$ with $\dot\theta_2$.

2. n > 3

For any n, the sum of angular velocities $\sum_i \dot\theta_i = \sum_i \omega_i \equiv n\Omega$. If synchronization occurs, all oscillators must therefore end up with the same constant angular speed, $\dot\theta_i = \Omega$, and the oscillators with their natural frequencies closest to Ω can be expected to reach this speed the earliest, considering the symmetry of the coupling. For odd n, if the ω_i's are chosen such that $\omega_{i+1} - \omega_i =$ constant for all $i < n$, then for the central oscillator, θ_k where $k = (n+1)/2$, first reaches a constant speed, $\dot\theta_k = \omega_k$ when ε is increased. When this occurs, from Eq. (5) with a little algebra, it can be seen that

$$\dot\theta_{k+i} - \dot\theta_k = \dot\theta_k - \dot\theta_{k-i}, \tag{15}$$

for any $i \leqslant k-1$.

For the case of $\sum_i \omega_i = 0$ in Eq. (5) that has been studied earlier [36], we impose the additional constraint $\Delta\omega_{i+1,i} = \omega_{i+1} - \omega_i$ is constant. Numerical results are presented for the case of $n = 15$ oscillators in Fig. 9 with $\omega_1 = -7$, $\Delta\omega_{i+1,i} = 1$ and $\varepsilon = 28$. As can be seen in Fig. 9, the central oscillator, $k = 8$, is stationary: $\dot\theta_k = 0$. Equation (15) then gives $\dot\theta_{k+1} = -\dot\theta_{k-1}$, $\dot\theta_{k+2} = -\dot\theta_{k-2}$, and so on. Thus, the curves for $\dot\theta_1$ and $-\dot\theta_n$ (dashed red) are identical, as are $\dot\theta_{k-1}$ and $-\dot\theta_{k+1}$ (dashed blue). Therefore, velocity extrema are identical for oscillator θ_i and oscillator θ_{n+1-i}, and phase slips are simultaneous for oscillator pairs $(\theta_i, \theta_{n+i-1})$. Note that they are not simultaneous among all oscillators in general: the slips for θ_1 and θ_n occur at S$_1$ and S$_2$, while for θ_{k-1} and θ_{k+1} they occur at S$'_1$.

This symmetry is maintained when n is even as well. During the approach to synchronization, the oscillator pairs move together, namely, $\dot\theta_i = \dot\theta_{n+1-i}$. Extrema of the phase velocity are thus also symmetric, and this results in temporal relationships between the phase slips in individual oscillators (results not shown).

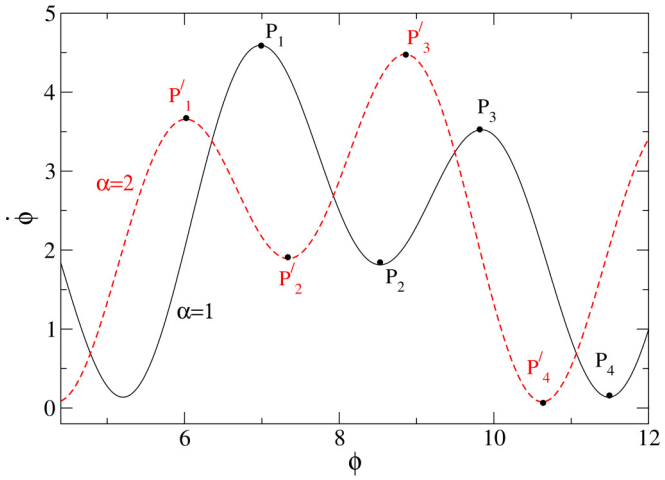

FIG. 10. For Eq. (18), a plot of $\dot{\phi}$ vs ϕ plots for $\alpha = 1$ (black) and for $\alpha = 2$ (dashed red) showing the perpetual points.

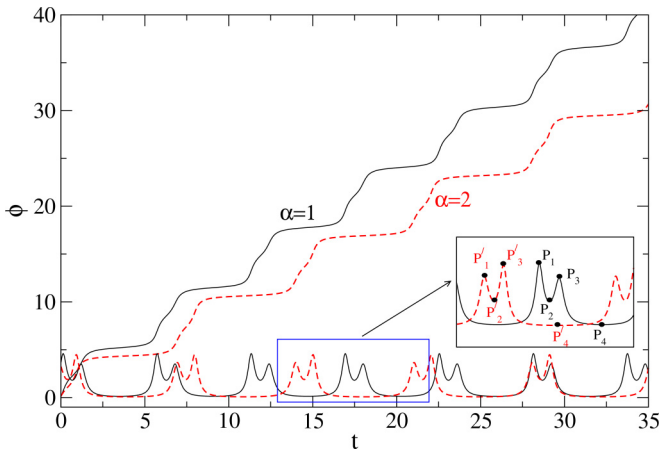

FIG. 11. ϕ and $\dot{\phi}$ as a function of time for Eq. (18) for the cases of $\alpha = 1$ (black) and for $\alpha = 2$ (dashed red) demonstrating phase slips at perpetual points; see Fig. 10.

III. OTHER COUPLING SCHEMES

To elucidate the role of stationary points, we consider a system that does not undergo a saddle-node bifurcation but has phase slips. Consider, for instance, a system of n phase oscillators with nearest-neighbor coupling of the form

$$\dot{\theta}_i = \omega_i - \left[\frac{\sin(\theta_{i+1}-\theta_i)}{2} + \frac{\sin(\theta_{i-1}-\theta_i)}{2}\right] + \frac{\varepsilon}{2}[-\sin^2(\theta_{i+1}-\theta_i+\alpha) + \sin^2(\theta_{i-1}-\theta_i-\alpha)], \tag{16}$$

where θ_i and ω_i are, respectively, the phase and the natural frequency of the ith oscillator, $i = 1, 2, 3, \ldots, n$. For $n = 2$, this becomes

$$\dot{\theta}_1 = \omega_1 - \frac{\sin(\theta_2-\theta_1)}{2} - \frac{\varepsilon}{2}\sin^2(\theta_2-\theta_1+\alpha),$$
$$\dot{\theta}_2 = \omega_2 - \frac{\sin(\theta_1-\theta_2)}{2} + \frac{\varepsilon}{2}\sin^2(\theta_1-\theta_2-\alpha). \tag{17}$$

Choosing $\omega_2 = 2$ and $\omega_1 = 1$ and defining $\phi = \theta_2 - \theta_1$ gives

$$\dot{\phi} = 1 + \sin\phi + \varepsilon\sin^2(\phi+\alpha). \tag{18}$$

For our analysis, we fix $\varepsilon = 3$, and choose the parameter being varied to be α. Note that there is no saddle-node bifurcation when α is varied in Eq. (18) irrespective of ε and, consequently, there are no saddle-node remnants. The relative positions of the perpetual points do change with α and this shifts the locations of the phase slips. Since $\dot{\theta}_1 + \dot{\theta}_2 = \omega_1 + \omega_2$ is constant, the relative dynamics between individual oscillators is similar to that seen in the Kuramoto oscillators, Eq. (7). The $\dot{\phi}$ vs ϕ plots in Fig. 10 for Eq. (18) present the four PPs for ϕ when $\alpha = 1$ (black curve): $0.70 \pm 2j\pi$ (P_1), $2.24 \pm 2j\pi$ (P_2), $-2.72 \pm 2j\pi$ (P_3), and $-1.08 \pm 2j\pi$ (P_4). Similarly, when $\alpha = 2$ (dashed-red curve) the four PPs are $-0.26 \pm 2j\pi$ (P'_1), $1.06 \pm 2j\pi$ (P'_2), $2.57 \pm 2j\pi$ (P'_3), and $-1.94 \pm 2j\pi$ (P'_4), where j is an integer. Phase slips occur at the faster PPs, P_1 and P_2 for $\alpha = 1$, and P'_1 and P'_2 for $\alpha = 2$, while dynamics is sticky around P_4 and P'_4; see Fig. 11.

Thus, even in the absence of a saddle-node bifurcation, phase slips occur, and their locations can be directly correlated with the velocity extrema or perpetual points.

We further consider another form of the coupling which is similarity dependent [48], with an inverse dependence on the phase distance. Thus the coupling strength is maximal when the phase variables are identical and minimal when they are the most dissimilar. Such couplings arise naturally in mobile systems such as swarmalators [50] and has been shown to induce extreme events as well as to facilitate inhomogeneous limit cycles to oscillation death transitions in coupled oscillators [48,51]. A simple example of such coupling is given as

$$\dot{\theta}_i = \omega_i + \frac{\varepsilon}{2}\left[-\frac{1}{\alpha - \cos(\theta_{i+1}-\theta_i)} + \frac{1}{\alpha - \cos(\theta_{i-1}-\theta_i)}\right], \tag{19}$$

where θ_i and ω_i are the phase and natural frequency of the ith oscillator, and $\alpha > 1$. For $n = 2$, we then have

$$\dot{\theta}_1 = \omega_1 - \varepsilon\left[\frac{1}{\alpha - \cos(\theta_2-\theta_1)}\right],$$
$$\dot{\theta}_2 = \omega_2 + \varepsilon\left[\frac{1}{\alpha - \cos(\theta_1-\theta_2)}\right]. \tag{20}$$

The coupling in Eq. (20) has maximum strength when $\theta_2 - \theta_1 = 0$ and is weakest when $\theta_2 - \theta_1 = \pi$. For the phase difference, $\phi = \theta_2 - \theta_1$, we now have

$$\dot{\phi} = (\omega_2 - \omega_1) + 2\varepsilon\left[\frac{1}{\alpha - \cos\phi}\right]. \tag{21}$$

For $\omega_2 = \omega_1 - 0.3$, $\alpha = 1.1$, and $\varepsilon = 0.32$, the evolution of ϕ and $\dot{\phi}$ are depicted in Fig. 12. Solving for $\ddot{\phi} = 0$ in Eq. (21) gives two perpetual points: $\phi = 0$ and $\phi = \pi$ denoted P_1 and P_2, respectively, in Fig. 12. From the evolution curve for ϕ (black curve) in the figure, it is apparent that ϕ undergoes slips at the fast perpetual points P_1, which signifies asynchrony between the individual oscillators, and remains almost constant around the slow perpetual point, P_2, signifying short-time synchronization. Additionally, because of the

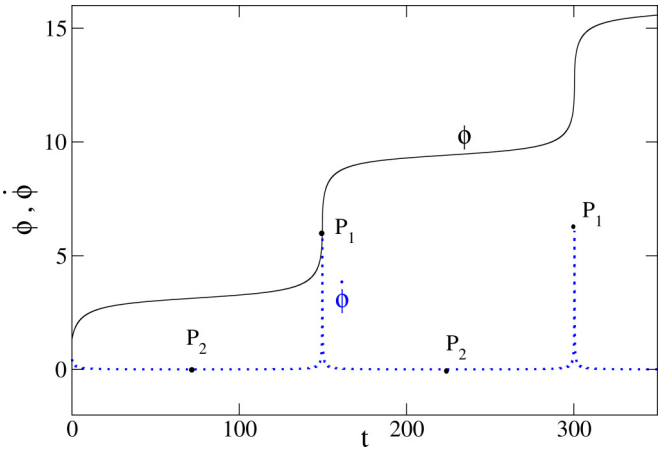

FIG. 12. Phase ϕ (black) and velocity $\dot{\phi}$ (dotted blue) as a function of time for Eq. (21) for parameters $\omega_2 - \omega_1 = -0.3$, $\alpha = 1.1$, and $\varepsilon = 0.32$.

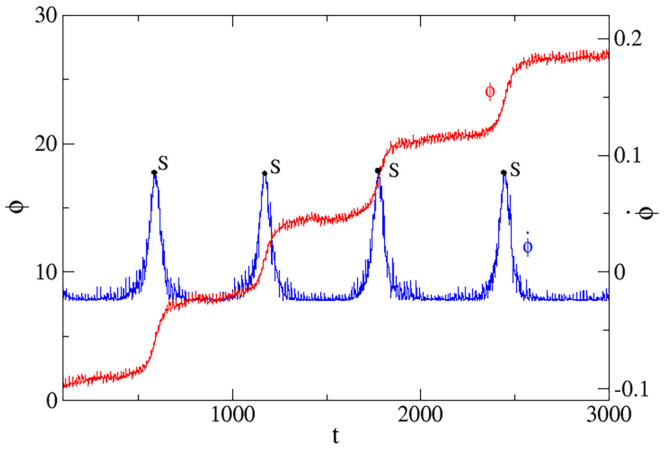

FIG. 13. Slips in the phase difference, ϕ, between the coupled Rössler oscillators (solid-red curve), Eq. (22), compared with the evolution of the velocity (blue curve), $\dot{\phi}$.

similarity-dependent nature of the coupling, the phase slips in this case occur whenever the two oscillators cross each other.

IV. COUPLED CHAOTIC SYSTEMS

Phases are not uniquely defined in chaotic systems: these are typically calculated from any associated observable through a Hilbert transform. When two chaotic systems are coupled, phase synchronization occurs as the systems transition from a state where their Hilbert phases θ_1 and θ_2 move with different velocities to a synchronous state where their phase differences satisfy a weak locking condition $|\theta_1 - \theta_2| < C$ [4]. This route to synchronization, as in the case of phase oscillators, is observed to be characterized by phase slips. By analyzing the reduced dynamics of these phases for the cases of two coupled Rössler and hyperchaotic Rössler systems, we confirm the role of stationary points of velocities in phase slips in these systems.

A. Coupled Rössler systems

We first consider two coupled Rössler oscillators,

$$\begin{aligned} \dot{x}_{1,2} &= -\omega_{1,2} y_{1,2} - z_{1,2} + \varepsilon(x_{2,1} - x_{1,2}), \\ \dot{y}_{1,2} &= \omega_{1,2} x_{1,2} + 0.15 y_{1,2}, \\ \dot{z}_{1,2} &= 0.2 + z_{1,2}(x_{1,2} - 10), \end{aligned} \tag{22}$$

where phase slips occur when there is a mismatch between the frequencies $\omega_{1,2}$ [4].

In general, the evolution of the phase for an autonomous chaotic oscillator can be described by an equation of the form

$$\dot{\theta} = \omega + F(A), \tag{23}$$

where ω is the mean frequency and $F(A)$ the amplitude-dependent part. For Eq. (22), this leads to, with further simplifications, the following expression for the evolution of their phase difference $\phi = \theta_1 - \theta_2$:

$$\dot{\phi} = \omega_1 - \omega_2 - 2\varepsilon \sin(\phi) + F_1(A_1) - F_2(A_2). \tag{24}$$

Now, since in the Rössler attractor the amplitude dependence of frequency is small, the term $F_1(A_1) - F_2(A_2)$ can be neglected and Eq. (24) becomes similar to Eq. (7), which describes two coupled phase oscillators [4]. We show this in Fig. 13 for the case $\omega_{1,2} = 1 \pm 0.015$. The slips in the phase difference ϕ (red curve) occur at the maxima of $\dot{\phi}$ (marked as S on the blue curve), at $\phi \approx (3\pi/2 \pm 2j\pi)$, and the correspondence is identical to that of Fig. 2(a).

B. Coupled hyperchaotic Rössler systems

Phase slips are also observed in two coupled hyperchaotic Rössler oscillators,

$$\begin{aligned} \dot{x}_{1,2} &= -\omega_{1,2} y_{1,2} - z_{1,2} + \varepsilon(x_{2,1} - x_{1,2}), \\ \dot{y}_{1,2} &= \omega_{1,2} x_{1,2} + 0.25 y_{1,2} + w_{1,2}, \\ \dot{z}_{1,2} &= 3.0 + x_{1,2} z_{1,2}, \\ \dot{w}_{1,2} &= -0.5 z_{1,2} + 0.05 w_{1,2} + \varepsilon(w_{2,1} - w_{1,2}), \end{aligned} \tag{25}$$

with a parameter mismatch $\omega_{1,2} = 1 \pm 0.0005$ [52].

After a little algebra, the evolution of the phase difference $\phi = \theta_1 - \theta_2$ can be derived as [52]

$$\dot{\phi} = \Delta\omega + a \sin\phi + b \sin\frac{\phi}{2} + \eta, \tag{26}$$

where

$$\begin{aligned} \Delta\omega &= \omega_1 - \omega_2, \\ a &= (0.25 + \varepsilon)\cos(\theta_1 + \theta_2) - \frac{\varepsilon}{2}\left(\frac{A_1}{A_2} + \frac{A_2}{A_1}\right), \\ b &= 2\left(\frac{z_1}{A_1}\cos\left(\frac{\theta_1 + \theta_2}{2}\right) - \frac{w_1}{A_1}\sin\left(\frac{\theta_1 + \theta_2}{2}\right)\right), \\ \eta &= \left(\frac{z_1}{A_1} - \frac{z_2}{A_2}\right)\sin\theta_2 + \left(\frac{w_1}{A_1} - \frac{w_2}{A_2}\right)\cos\theta_2, \\ &\quad - \frac{\varepsilon}{2}\left(\frac{A_2}{A_1} - \frac{A_1}{A_2}\right)\sin\left(\theta_1 + \theta_2\right). \end{aligned} \tag{27}$$

Since a and b are fast fluctuating variables, their time averages can be considered in Eq. (26) and a simplified expression

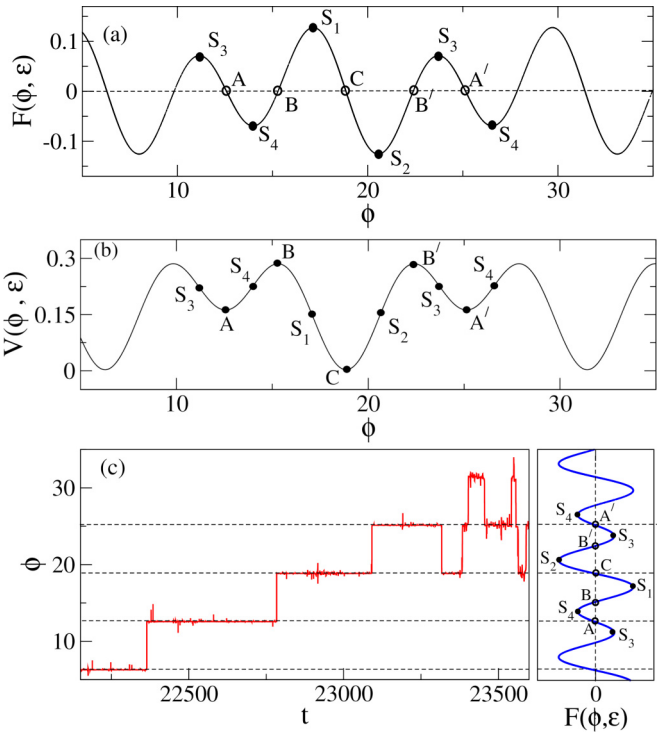

FIG. 14. For the coupled hyperchaotic Rössler oscillators, Eqs. (25), with $\varepsilon = 0.16$, (a) $F(\phi, \varepsilon)$ vs ϕ [see Eq. (29)] and (b) $V(\phi, \varepsilon)$ vs ϕ [see discussion after Eq. (29)]. In (c), phase ϕ is shown as a function of time (solid-red line) in the left panel while the right panel shows (a) rotated by 90°, with the extrema S_k, and points A, B, C, A′, and B′ being marked (see text). The horizontal dashed lines in (c) are a guide to the eye to visualize the phase slips of $\pm 2\pi$, which may occur, for example, from A to C ($+2\pi$) or from A′ to C (-2π).

can be obtained,

$$\dot{\phi} = F(\phi, \varepsilon) + \eta, \tag{28}$$

where

$$F(\phi, \varepsilon) = \Delta\omega + \langle a \rangle \sin\phi + \langle b \rangle \sin\frac{\phi}{2}, \tag{29}$$

with $\langle \cdot \rangle$ denoting time averages. The additional term η in this case causes the irregularities in the phase-slip structure, as shown in Fig. 14(c) (solid-red curve) for $\varepsilon = 0.16$. The phase slips here are induced by a combined effect of the perturbative term and the extrema of $F(\phi, \varepsilon)$. For an illustration, we plot $F(\phi, \varepsilon)$ and the corresponding potential $V(\phi, \varepsilon)$ $[= -\int^{\phi} F(\phi', \varepsilon)\, d\phi']$ against ϕ in Figs. 14(a) and 14(b), respectively. The extrema of $F(\phi, \varepsilon)$ are marked as S_1, S_2, S_3, and S_4. Consider the system at A, at the bottom of a well, in Fig. 14(b). It sticks around A until fluctuations dislodge it to the left or to the right. If it is perturbed to the right, past S_4 and beyond B, it *slips* past S_1 and settles at C, which results in a net shift of $+2\pi$. On the other hand, if it is pushed to the left, from point A′, for example, slippage occurs across S_2, resulting in a -2π shift, with the system again ending up at C. The correlation is apparent from the correspondence between ϕ vs $F(\phi, \varepsilon)$ (dotted blue) and ϕ vs t (solid red) curves as presented in Fig. 14(c).

The above analysis for Rössler and hyperchaotic Rössler systems therefore verifies the role of stationary points in inducing phase slips in oscillators in general.

V. SUMMARY

In this paper, we have investigated two basic aspects of phase slips: why they occur and where they are located. Our study shows that both involve the stationary points of *velocities*. The temporal relation between the slips in individual oscillators is not as straightforward as previously thought [36], and under a general setting phase slips are in fact typically nonsimultaneous. The analysis complements the treatment of the cascade of phase slips and phase synchronization being a consequence of the saddle-node ghost [36,37].

By systematically investigating two-, three-, and n-coupled phase oscillators, we establish the causal relationship between stationary points of the velocities and phase slips. The relative positions of these points dictate where phase slips occur, and the corresponding velocity magnitudes decide to what extent they occur. The same mechanism is responsible for phase slips in systems where saddle-node bifurcations are absent, as we show for a modified system [Eq. (9)]. Its presence when the form of coupling is altered, such as for the case of similarity-dependent coupling [Eq. (19)], further establishes its generality.

The ideas presented in this paper find relevance well beyond the case of phase oscillators. Stationary points locate phase slips in coupled chaotic systems involving amplitudes, which we have verified for two coupled Rössler systems and for two coupled hyperchaotic Rössler systems. They may also be used to describe phase slips observed in coupled, structurally nonequivalent systems, which are important in various physical and biological fields [53]. The observed asynchrony between phase slips in individual phase oscillators described by these points can moreover be linked to the unsynchronised phase slips observed in coupled, forced chaotic systems [54]. Other possible applications include analyzing outputs of semiconductor laser arrays and chaotic maps [4,49,55].

Given the current interest in complex networks, a promising direction for future research would be to extend the present analysis to topologically different networks of coupled chaotic systems. A detailed study of the temporal relationship between phase slips among the individual oscillators in such networks should be of considerable interest.

ACKNOWLEDGMENTS

P.B.G. acknowledges financial support from the University of Delhi through the University Research Fellowship. S.K. acknowledges the Center for Nonlinear Systems, Chennai Institute of Technology (CIT), India, vide Funding No. CIT/CCM/2023/RP-016. A.P. thanks the IoE, University of Delhi for financial support.

[1] L. M. Pecora and T. L. Carroll, Phys. Rev. Lett. **64**, 821 (1990).
[2] A. Pikovsky, M. Rosenblum, and J. Kurths, *Synchronization: A Universal Concept in Nonlinear Sciences* (Cambridge University Press, New York, 2002).
[3] A. Pikovsky, M. Rosenblum, and J. Kurths, Am. J. Phys. **70**, 655 (2002).
[4] M. G. Rosenblum, A. S. Pikovsky, and J. Kurths, Phys. Rev. Lett. **76**, 1804 (1996).
[5] D. Pazo, M. Zaks, and Z. Kurths, Chaos **13**, 309 (2003).
[6] S. Boccaletti, A. N. Pisarchik, C. I. Del Genio, and A. Amann, *Synchronization: From Coupled Systems to Complex Networks* (Cambridge University Press, Cambridge, 2018).
[7] H. Nakao, Contemp. Phys. **57**, 188 (2016).
[8] A. N. Pisarchik, *Recent Advances in Laser Dynamics: Control and Synchronization* (Research Signpost, Kerala, 2008).
[9] K. Wiesenfeld, P. Colet, and S. H. Strogatz, Phys. Rev. Lett. **76**, 404 (1996).
[10] K. Wiesenfeld, P. Colet, and S. H. Strogatz, Phys. Rev. E **57**, 1563 (1998).
[11] V. Makarenko and R. Llinás, Proc. Natl. Acad. Sci. USA **95**, 15747 (1998).
[12] P. Tass, M. G. Rosenblum, J. Weule, J. Kurths, A. Pikovsky, J. Volkmann, A. Schnitzler, and H. J. Freund, Phys. Rev. Lett. **81**, 3291 (1998).
[13] U. Parlitz, L. Junge, W. Lauterborn, and L. Kocarev, Phys. Rev. E **54**, 2115 (1996).
[14] P. K. Roy, S. Chakraborty, and S. K. Dana, Chaos **13**, 342 (2003).
[15] C. Schäfer, M. G. Rosenblum, J. Kurths, and H. H. Abel, Nature **392**, 239 (1998).
[16] P. A. Tass, Biol. Cybern. **89**, 81 (2003).
[17] B. Blasius, A. Huppert, and L. Stone, Nature **399**, 354 (1999).
[18] J. Sharma, I. Tiwari, D. Das, P. Parmananda, V. S. Akella, and V. Pimienta, Phys. Rev. E **99**, 012204 (2019).
[19] R. Jain, J. Sharma, I. Tiwari, S. D. Gadre, S. Kumarasamy, P. Parmananda, and A. Prasad, Phys. Rev. E **106**, 024201 (2022).
[20] A. Arenas, A. Díaz-Guilera, J. Kurths, Y. Moreno, and C. Zhou, Phys. Rep. **469**, 93 (2008).
[21] C. Li and G. Chen, Physica A **341**, 73 (2004).
[22] A. Keane, A. Neff, K. Blaha, A. Amann, and P. Hövel, Chaos **33**, 063133 (2023).
[23] M. Brede and A. C. Kalloniatis, Phys. Rev. E **93**, 062315 (2016).
[24] M. Sarkar, and N. Gupte, Phys. Rev. E **103**, 032204 (2021).
[25] R. E. Amritkar and S. Jalan, Physica A **321**, 220 (2003).
[26] B. Scholz-Reiter, J. T. Tervo, and M. Freitag, Physica A **363**, 32 (2006).
[27] H. Yu, J. Wang, B. Deng, X. Wei, Y. K. Wong, W. L. Chan, K. M. Tsang, and Z. Yu, Chaos **21**, 013127 (2011).
[28] Y. Kuramoto, *Chemical Oscillations, Waves, and Turbulence* (Springer Series in Synergetics, Berlin, Heidelberg, 1984).
[29] S. H. Strogatz, Physica D **143**, 1 (2000).
[30] F. Dörfler and F. Bullo, Automatica, **50**, 1539 (2014).
[31] D. J. Klein, P. Lee, K. A. Morgansen, and T. Javidi, IEEE J. Sel. Areas Commun. **26**, 695 (2008).
[32] D. A. Paley, N. E. Leonard, R. Sepulchre, D. Grunbaum, and J. K. Parrish, IEEE Control Syst. Magazine **27**, 89 (2007).
[33] R. Sepulchre, D. A. Paley, and N. E. Leonard, IEEE Trans. Automat. Contr. **52**, 811 (2007).
[34] N. Ainsworth, and S. Grijalva, IEEE Trans. Power Syst. **28**, 4310 (2013).
[35] L. Buzna, S. Lozano, and A. Diaz-Guilera, Phys. Rev. E **80**, 066120 (2009).
[36] Z. Zheng, G. Hu, and B. Hu, Phys. Rev. Lett. **81**, 5318 (1998).
[37] S. H. Strogatz, *Nonlinear Dynamics and Chaos* (Westview Press, Boulder, Colorado, 2015).
[38] A. Prasad, Int. J. Bifurcation Chaos **25**, 1530005 (2015).
[39] N. Kuznetsov, O. Kuznetsova, G. Leonov, T. Mokaev, and N. Stankevich, IFAC-PapersOnLine **50**, 2651 (2017), 20th IFAC World Congress.
[40] G. Leonov, N. Kuznetsov, and V. Vagaitsev, Phys. Lett. A **375**, 2230 (2011).
[41] A. P. Kuznetsov, S. P. Kuznetsov, E. Mosekilde, and N. V. Stankevich, J. Phys. A: Math. Theor. **48**, 125101 (2015).
[42] D. Dudkowski, A. Prasad, and T. Kapitaniak, Chaos **26**, 103103 (2016).
[43] P. Brzeski and L. N. Virgin, Nonlinear Dyn. **90**, 2917 (2017).
[44] P. Brzeski and L. Virgin, Mech. Syst. Signal Process. **108**, 115 (2018).
[45] S. Kumarasamy, D. Dudkowski, A. Prasad, and T. Kapitaniak, Chaos **31**, 081102 (2021).
[46] A. Hastings, Ecol. Lett. **4**, 215 (2001).
[47] O. Ovaskainen and I. Hanski, Theor. Popul Biol. **61**, 285 (2002).
[48] P. B. Gogoi, S. Kumarasamy, A. Prasad, and R. Ramaswamy, Chaos **32**, 113138 (2022).
[49] K. Arai and S. Mizutani, Proc. SPIE **5471**, 492 (2004).
[50] K. P. O'Keeffe, H. Hong, and S. H. Strogatz, Nat. Commun. **8**, 1504 (2017).
[51] S. Kumarasamy, S. Srinivasan, P. B. Gogoi, and A. Prasad, Commun. Nonlinear Sci. Numer. Simul. **107**, 106170 (2022).
[52] C. M. Kim, W. H. Kye, I. B. Kim, Y. J. Park, AIP Conf. Proc. **501**, 181 (2000).
[53] J. Y. Chen, K. W. Wong, and J. W. Shuai, Chaos **12**, 100 (2002).
[54] S. Mizutani, K. Arai, and P. Davis, *International Symposium on Nonlinear Theory and its Applications (NOLTA2004) Fukuoka*, Japan, Nov. 29–Dec. 3 (Institute of Electronics, Information and Communication Engineers, 2004).
[55] H. G. Winful and L. Rahman, Phys. Rev. Lett. **65**, 1575 (1990).